



RESEARCH ARTICLE

WILEY

A geometrical method for quantifying endmembers' fractions in three-component groundwater mixing

Emilio Cuoco^{1,2}  | Stefano Viaroli³  | Thomas H. Darrah^{4,5} | Vittorio Paolucci⁶ | Roberto Mazza³ | Dario Tedesco^{1,2}

¹Istituto Nazionale di Geofisica e Vulcanologia - Osservatorio Vesuviano (INGV-OV), Naples, Italy

²Dipartimento di Scienze e Tecnologie Ambientali, Biologiche e Farmaceutiche, Università della Campania "Luigi Vanvitelli", Caserta, Italy

³Dipartimento di Scienze, Università degli Studi Roma Tre, Rome, Italy

⁴School of Earth Sciences, The Ohio State University, Columbus, Ohio, USA

⁵Global Water Institute, The Ohio State University, Columbus, Ohio, USA

⁶Ferrarelle S.p.A., Riardo, Italy

Correspondence

Emilio Cuoco, Istituto Nazionale di Geofisica e Vulcanologia - Osservatorio Vesuviano (INGV-OV), Via Diocleziano 328, Naples, Italy.
Email: emilio.cuoco@ingv.it

Abstract

We present a new geometrical method capable of quantifying and illustrating the outcomes of a three-component mixing dynamics. In a three-component mixing scenario, classical algebraic equations and endmember mixing analysis (EMMA) can be used to quantify the contributions from each fraction. Three-component mixing of natural waters, either in an element–element plot or by using the EMMA mixing subspace is described by a triangular shaped distribution of sample points where each endmember is placed on an apex, while each side corresponds to the mixing function of the two endmembers placed at the apex, considering the third endmembers' contribution equal to zero. Along each side, the theoretical mixing fractions can be computed using mass balance equations. Samples with contributions from three endmembers will plot inside the triangle, while the homogeneous barycentric coordinate projections can be projected onto the three sides. The geochemistry observed in the mineralized Ferrarelle aquifer system (southern Italy) results from three-component mixing of groundwater, each with diagnostic geochemical compositions. The defined boundary conditions allow us to parameterize and validate the procedures for modelling mixing, including selection of suitable geochemical tracers.

KEYWORDS

Ferrarelle groundwater system, geochemistry, groundwater chemistry, quantitative geoscience, three-component mixing

1 | INTRODUCTION

Mixing between different sources of water is one of the most common and important hydrological process in nature (e.g., Barros Grace et al., 2008; Domenico & Schwartz, 1997; Ramón et al., 2021; Stegen et al., 2016; Wilson et al., 2016). The definition of the endmembers of the mixing allows to understand the hydrodynamics and the chemical processes.

The results of these mixing processes can sometimes influence water quality limiting water access due to the presence of lower

quality water mixtures. The worsening of the original groundwater composition could be related to natural contaminations (uprising of deep geothermal fluids rich in arsenic (As), iron (Fe), or other trace metals or hydrocarbons, Bundschuh & Maity, 2015; Donato et al., 2021; Tassi et al., 2009) or due to leaching of shallow aquifers contaminated by human activities (pesticides and fertilizers in agricultural areas or wastewaters in urban areas, Li et al., 2021; Mateo-Sagasta et al., 2017). As a result of these processes, the final composition of a mixed parcel of water can be complex and depends on the relative concentrations and percentage of each mixing component.

This is an open access article under the terms of the Creative Commons Attribution License, which permits use, distribution and reproduction in any medium, provided the original work is properly cited.

© 2021 The Authors. *Hydrological Processes* published by John Wiley & Sons Ltd.

The investigation of hydrological processes related to the groundwater mixing dynamics can be especially important in complex hydrogeological systems, where vertical and/or lateral groundwater exchanges occur between different aquifers, or where the lack of data limits the understanding of deep aquifer dynamics.

The effect on solute concentrations during mixing are traditionally described using mathematical models (e.g., Christophersen & Hooper, 1992; Mazar et al., 1993; Schramke et al., 1996). Using these methods, algebraic modelling can be used to quantitatively determine the fractions of original water (endmember) and added components that were contributed to the sample mixture. More recently developed mixing models (Hooper, 2003; Liu et al., 2017) are based on computational linear algebra, known as end member mixing analysis (EMMA). The EMMA method is widely employed for exploration of complex hydrological systems (James & Roulet, 2006; Katsuyama et al., 2001; Kronholm & Capel, 2014; Liu et al., 2008), as well as groundwater systems in which chemical reactions occurring in a diverse range of hydrogeological settings are of great significance (Pelizardi et al., 2017).

Robust detection and modelling of groundwater mixing processes will allow the improvement of hydrogeological conceptual modelling and improve the understanding of groundwater geochemistry, which are important first steps in more elaborate investigations on water (e.g., water budget calculation, evaluation of potential contamination from external sources). The ability to improve conceptual models is an important tool for developing proper management strategies, especially in mineralized aquifers tapped for bottling activity, where the healthiness and the constancy of the groundwater chemical composition must be guaranteed (Europe Directive 2009/54/EC). When endmembers mix conservatively the mixture, geometrically, will lie in the convex set where the vertices are the three components (Christophersen & Hooper, 1992 and therein references). In case of a three component mixing, the set corresponds to a triangle on the plane defined by the three endmembers. This triangle can act as reference triangle in a homogeneous barycentric coordinate system.

In the present investigation we test a new and fast geometrical method to quantify the relative mixing fractions of three endmembers directly from the bidimensional mixing space. This method can be applied both for the endmember fractions estimations based on the simple mass balance equations and for the multivariate EMMA method.

The proposed method was tested on the Ferrarelle groundwater system (FGS), a complex mineral system strictly governed by groundwater mixing (Cuoco et al., 2020). Despite the complex and peculiar hydrogeological setting, the studied system is supported by an extensive bibliographic knowledge (Sacchi et al., 2021 and reference therein) and a robust monthly chemical dataset. Specifically, the water chemistry reflects a balance between recently entrained volcanically influenced waters and carbonate aquifers (Cuoco et al., 2010). Upflow of CaCO_3 and CO_2 rich groundwater occurs from the deep confined carbonate aquifer through the fault systems, which greatly influence the sedimentary bedrock and allow mixing with less mineralized groundwater in the volcanic aquifer (Corniello et al., 2015; Cuoco

et al., 2017; Cuoco, Darrah, Buono, Eymold, & Tedesco, 2015; Cuoco, Viaroli, Paolucci, et al., 2021). Cuoco et al. (2020) and Cuoco, Viaroli, Paolucci, et al. (2021) argued for the presence of a third groundwater component in the FGS, which was hypothesized to result from mixing by lateral inflow from the Mt. Maggiore region. This third component is dominantly alkali earth-bicarbonate-type water with low total dissolved solids. Thus, Cuoco et al. (2020) concluded that the FGS geochemistry is defined by three-component groundwater mixing. The three recognized endmembers are: (i) the deep and highly mineralized groundwater from the carbonate basement, (ii) shallower volcanically influenced waters with low degrees of mineralization and (iii) lateral alkali earth-bicarbonate type from a nearby high-relief carbonate platform. In summary, in the present investigation we (i) test a new geometrical method which can be considered as a useful tool for quantifications of endmember fractions in three-component mixing processes of natural waters. In addition, the visualization of the result on a ternary diagram allows the comparison between each sample in term of different mixing fractions. (ii) We point out some experimental evidence useful to evaluate a chemical variable as effective tracer in hydrological processes. In addition, (iii) we provide a numerical parametrization of the groundwater mixing of the FGS. The proposed method may be useful also as support for a more aware exploitation of mineralized groundwater resources.

2 | STUDY AREA

2.1 | Geological setting

The study area is located within the Riardo Plain along the northern flank of the Mt. Maggiore ridge in the northern Campania Region of southern Italy. This area consists of two main geological settings: marine sedimentary sequences and volcanites that erupted from the Roccamonfina volcano (Figure 1a).

The sedimentary basement corresponds to the Meso-Cenozoic Apennine carbonate sequence. These units have been heavily deformed by various orogenic phases since the Miocene and later during the Plio-Pleistocene extension, which displaced the basement via horst and graben structures (Boncio et al., 2016; Cosentino et al., 2006; Giordano et al., 1995). The Meso-Cenozoic carbonate units crop out both in the Mt. Maggiore (D'Argenio & Pescatore, 1962) and in the other mountain ridges that surround the Riardo Plain. Following deformation during the Apennine orogeny, the carbonate deposition ended and gave way to the deposition of marl and synorogenic flysch units. The flysch units are not deposited or preserved continuously as both processes were controlled by the presence of localized graben structures throughout the Riardo Plain (Saroli et al., 2014), whereas horsts are zones of either non-deposition or erosion.

The volcanic sequences within the Riardo Plain can be summarized as a sequence of loose layered pyroclastic and reworked volcanoclastic deposits from the Roccamonfina volcano (Viaroli, Lotti, et al., 2019) with alternating deposition of the Brown Leucitic Tuff

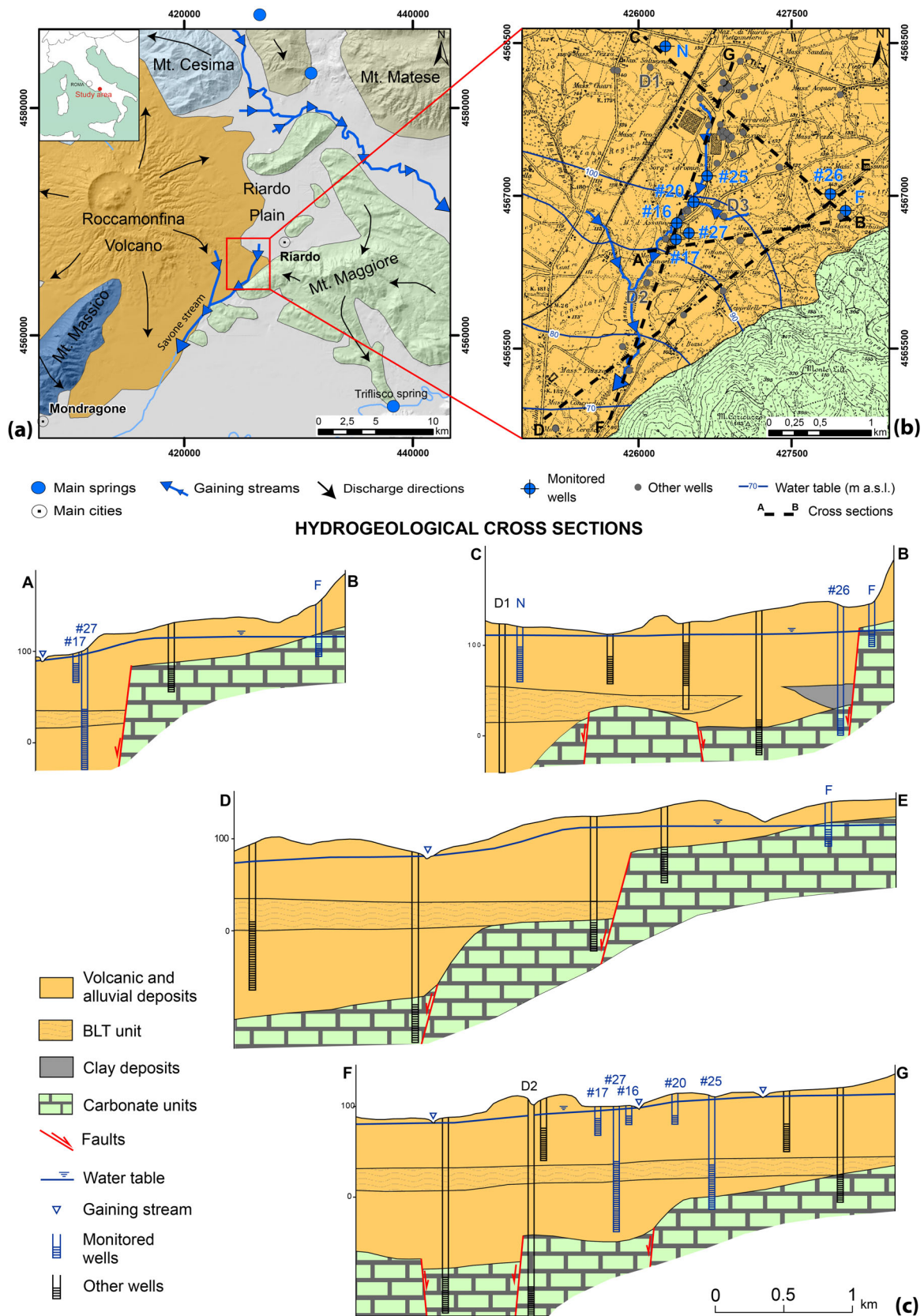


FIGURE 1 (a) Scheme of the regional aquifers in the study area (modified from Boni et al., 1986; Celico, 1978; Lancia et al., 2020); (b) Location of the available boreholes and the monitored wells in the Ferrarelle mineral water claim area; (c) Hydrogeological cross sections of the study area. The ID codes of sampled wells (in blue) are taken from Cuoco et al. (2020)

unit, which is a lithic tuff composed of an ash matrix (Luhr & Giannetti, 1987) (Figure 1c). Petrographic analysis carried out on cutting samples from boreholes in the Ferrarelle area (Università degli Studi Roma Tre, 1996, technical report) indicate the presence of several clay minerals (i.e., Halloysite 10 Å, Smectite, Chabazite and Illite) derived from the weathering of the volcanic glasses.

2.2 | Hydrogeological setting

The hydrogeological frameworks of the Riardo Plain, Roccamonfina Volcano and Mt. Maggiore were previously described at regional (Boni et al., 1986; Celico, 1978; De Vita et al., 2018; Viaroli et al., 2018) and local (Capelli et al., 1999; Mazza et al., 2013; Viaroli et al., 2016; Viaroli, Di Curzio, et al., 2019) scales. A relevant summary is included here for brevity.

The basal aquifer of the Roccamonfina volcano shows a radial drainage pattern towards the plains that surround the volcano edifice. Groundwater in this aquifer is mainly discharged through the Savone gaining stream with a mean discharge of $\sim 0.5 \text{ m}^3/\text{s}$ (Boni et al., 1986). The Mt. Maggiore aquifer feeds the Triflisco Spring, located at the southern side of the carbonate structure at an elevation of $\sim 30 \text{ m a.s.l.}$ with a mean discharge of $\sim 2.8 \text{ m}^3/\text{s}$ (Boni et al., 1986) (Figure 1a).

In the Riardo Plain, the hydrogeological framework is quite complex and heterogeneous. In the western Riardo Plain, the absence of intermediate aquiclude units allows for the upwelling of deeply source mineralized fluids along faults affecting the sedimentary basement, which leads to mixing between the shallow volcanically influenced groundwater (*N* component) and the more deeply sourced and highly mineralized carbonate aquifer (*D* component), the latter of which is responsible for creating the Ferrarelle mineral springs (Cuoco et al., 2010, 2020; Sacchi et al., 2021). The mineralization of groundwater varies locally (well to well) with groundwater chemistry varying according to the proximity of faults. While local chemistry is governed by discrete localized zones of fault-controlled fluid migration, the vast majority of data from the study area fall along an apparent two-component mixing line between volcanically influenced groundwater and the more deeply sourced and highly mineralized carbonate aquifer (Cuoco et al., 2020). Recent publications, Cuoco et al. (2020) identified the presence of an additional contribution in the mineral water mixing, corresponding to a lateral inflow from the phreatic carbonate aquifer of Mt. Maggiore (*F* component), however the relevance of this contribution in the groundwater mixing is not yet defined.

3 | MATERIALS AND METHODS

3.1 | Field measurements

Monitoring and sampling activities were performed monthly between October 2017 and January 2019 on eight monitoring wells placed within Ferrarelle™ company's water concession in the Riardo Plain (blue dots in Figure 1b). Groundwater depth was measured in the

piezometers where the static condition of the aquifer was well established. Groundwater depth was also measured daily in two monitoring wells (*N* and *F* in Figure 1b) using automatic probes (Schlumberger DIVER) during the same period (~ 18 months). The *N* and *F* monitoring wells tap the volcanic aquifer in the Riardo Plain and the carbonate non-mineralized aquifer of Mt. Maggiore, respectively, in order to evaluate the relationship between the aquifers during long-term monitoring. On average, the hydraulic heads measured in the mixing area were $\sim 100\text{--}115 \text{ m a.s.l.}$ (Figure 1c).

Field measurements were performed following the procedures described in Cuoco et al. (2020). Temperature, pH and electric conductivity (EC, with automatic compensation to 20°C) were measured in each surveyed point using portable probes (WTW pH/EC 340i). Precision and accuracy were determined for pH and EC by measuring relevant WTW certified standard solutions, the results were better than 1%. Redox potential (ORP) was measured in the field using a Hanna HI991002 meter with precision better than 5%.

3.2 | Chemical analysis

Major elements were analysed by ion chromatography on unacidified (*F*, *Cl*, *Br*, NO_3 and SO_4) and acidified (*Na*, *K*, *Mg* and *Ca*) samples. Bromide resulted always below detection limit. The total alkalinity (as HCO_3) was determined in the field (Kartell™ *technotrate* digital burette) by titration using standardized 0.1 M HCl (Merck™) against methyl orange indicator. All samples were filtered in the field using $0.45 \mu\text{m}$ Minisart sterile cellulose acetate membrane filters and then an aliquot was acidified ($\sim 1\%$) with ultra-pure Merck HNO_3 . Precision and accuracy for the IC analyses was tested by measuring certificated reference materials, confirming analytical error less than 7%. All reported water analyses show charge balances of less than $\pm 5\%$.

Trace metal analysis were carried out using Agilent 7500ce-ORS ICP-MS with collision cell technology according to the procedure described by Cuoco, Darrach, Buono, Verrengia, et al. (2015). Internal standards (constant concentration of ^{89}Y and ^{159}Tb) were used to monitor the instrumentation drift. External precision was monitored using an internal spike standard, which indicates errors of less than 10% for all reported analytes. All the trace metal analytes reported herein exceeded the limits of detection and quantification as calculated according to Long and Winefordner (1983) by at least an order of magnitude.

3.3 | Theoretical elements

In natural water systems, two or more sources of water can mix and change the resulting chemistry. Mixing can be described by an array of mathematical relationships (e.g., Albarede, 2009; Rutherford, 1994), including algebraic mass balances based on selected chemical variables (i.e., major ions, key elements). During mass balance approaches, the set of variables and equations are defined and used to determine mixing models that are used to quantitatively describe the hydrodynamics of groundwater systems.

The mixing between two different parcels of water is defined as 'two-component mixing' where each component, also called an endmember, represents the original composition of the unmixed solution. The concentrations of a conservative element in solution varies only according to dilution (or mixing with a more concentrated solution) and thus are not removed or enriched by chemical reactions. The concentration of conservative elements in a water solution produced by mixing of two-component (endmembers) α and β is given by the mass balance equation:

$$A_{\text{mix}} = f_{\alpha}A_{\alpha} + f_{\beta}A_{\beta} \quad (1)$$

where A is the concentration of the conservative element, which is now defined as a 'tracer', A_{mix} , A_{α} and A_{β} are respectively the concentrations of A in the mixed water, in α and β endmembers. If B is a second, different tracer, the mass balance can be also written:

$$B_{\text{mix}} = f_{\alpha}B_{\alpha} + f_{\beta}B_{\beta} \quad (2)$$

Considering that the sum of the fractions must be = 1:

$$f_{\beta} = 1 - f_{\alpha} \quad (3)$$

substituting Equation (3) in (1) and (2), and combining (1) and (2), the following relationship is obtained:

$$\frac{A_{\text{mix}} - A_{\beta}}{A_{\alpha} - A_{\beta}} = \frac{B_{\text{mix}} - B_{\beta}}{B_{\alpha} - B_{\beta}} \quad (4)$$

Relation (4) is the equation of a line in a Cartesian plane given from the coordinates of α and β (Figure 2a), where A_{mix} and B_{mix} are the variable concentrations of the two tracers in the water composition resulting from the mixing. In the Figure 2a the theoretical fractions (i.e., fixed fraction values) can be computed from Equations (1) and (2) and plotted on the line of the mixing function.

In a 'three-component mixing' scenario using the mass balance approach, three different water volumes, named α , β and γ , are assumed to mix each together. The mass balance equations are then defined by three fractions:

$$f_{\alpha} + f_{\beta} + f_{\gamma} = 1 \quad (5)$$

The mass balance needs to include two tracers (A_{mix} and B_{mix}) and can be solved as follows:

$$f_{\alpha}A_{\alpha} + f_{\beta}A_{\beta} + f_{\gamma}A_{\gamma} = A_{\text{mix}} \quad (6)$$

$$f_{\alpha}B_{\alpha} + f_{\beta}B_{\beta} + f_{\gamma}B_{\gamma} = B_{\text{mix}} \quad (7)$$

The algebraic solutions of (5), (6) and (7) give numerical values of the three fractions in the resulting water (Genereux, 1998; Liu et al., 2017). The geometric representation of the three-component mixing in a binary plot corresponds to a triangle (i.e., ternary diagram) (Figure 2b) whose vertices are defined by the coupled values of A and B tracers detected in the three endmembers. On the triangle surface, the water samples which are produced by the mix of the three endmembers can be plotted (Renner, 1988).

Fixing one of the three components equal to 0, the problem becomes a two-component mixing calculation (Figure 2a). As consequence, each side of the triangle can report the theoretical fractions of mixing related to the adjacent components (Figure 2b). From Equation (5) it is given by:

$$f_{\gamma} = 1 - f_{\beta} \quad \text{when} \quad f_{\alpha} = 0 \quad (8)$$

$$f_{\alpha} = 1 - f_{\gamma} \quad \text{when} \quad f_{\beta} = 0 \quad (9)$$

$$f_{\beta} = 1 - f_{\alpha} \quad \text{when} \quad f_{\gamma} = 0 \quad (10)$$

Considering Equation (8), the concentration C of a third conservative tracer in a generic solution b produced by the mixing of α and β endmembers is given by the following mass balance equation:

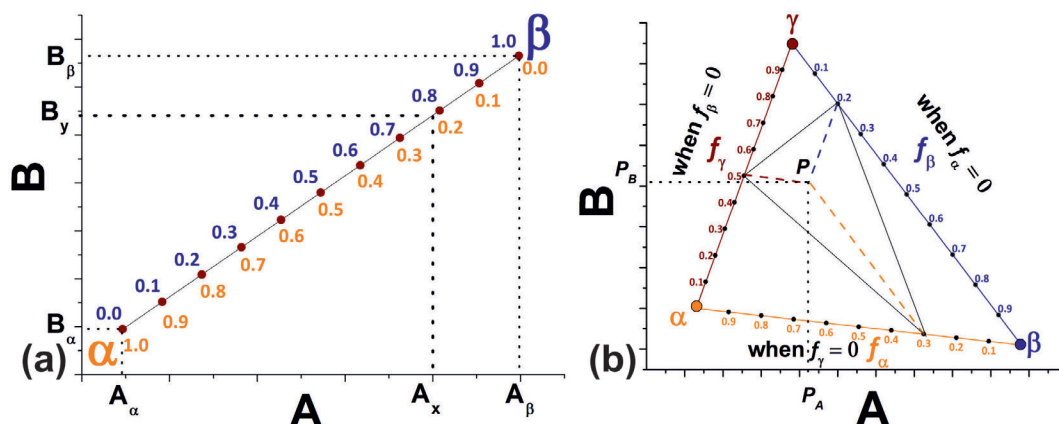


FIGURE 2 (a) A two-component mixing on an element–element plot. The theoretical fractions can be fixed and the corresponding coordinates can be computed through mass balance equations with the goal of reporting the references on the mixing line. (b) The plot shows a three-component mixing triangle where each endmember is placed on a different vertex. The theoretical mixing fractions has been computed by fixing the third endmember as equal to zero. A generic point P produced by a three-component mixing (P_A and P_B are given by chemical analyses) will be detected in a plot by the homogeneous barycentric coordinates systems, which allows one to show the quantification of each endmember on the corresponding side

$$C_b = f_\beta C_\beta + f_\gamma C_\gamma \quad (11)$$

similarly, from Equations (9) and (10) respectively:

$$C_c = f_\gamma C_\gamma + f_\alpha C_\alpha \quad (12)$$

$$C_a = f_\alpha C_\alpha + f_\beta C_\beta \quad (13)$$

In tracer–tracer plots, these equations are expressed in vectorial form (bold terms of the eq. stand for ‘vector’), with each concentration expressed by two-components related to tracers *A* and *B*.

Each side of the ternary diagram shown in Figure 2b reports the theoretical fractions of mixing computed considering the third endmember is equal to 0. For example, a water solution *P*, produced by the three-component mixing of α , β and γ , must fall within the ternary diagram (Figure 2b) and the fractions of each endmember are given by the homogeneous barycentric coordinates related to the theoretical fractions reported on each side of the ternary diagram:

$$C_p = C_\alpha f_\alpha + C_\beta f_\beta + C_\gamma f_\gamma \quad (14)$$

being $f_\alpha + f_\beta + f_\gamma = 1$ (Lidberg, 2011). The convex combination of the theoretical fractions on the ternary diagram detects the relative concentration of the α , β and γ endmembers which form the *P* solution.

In the example of the Figure 2b the position of *P* is defined through coordinates given by the triple of numbers ($f_\alpha : f_\beta : f_\gamma$) in the specific example is (0.3: 0.2: 0.5) in a given triangle $\alpha\beta\gamma$.

If we imagine the f_α , f_β and f_γ as masses, β and γ will balance at the point $X = \frac{f_\beta C_\beta + f_\gamma C_\gamma}{f_\beta + f_\gamma}$ which lie on the $\beta\gamma$ line. If we consider the two component mixing β versus γ the $f_\beta + f_\gamma = 1$ and the centre of masses *X* will be exactly the mass balance between β and γ . Taking the third component α , *X* will balance in a new centre of mass with α through the masses ($f_\beta + f_\gamma$) and f_α in the point *P*, thus we obtain $P = \frac{f_\alpha C_\alpha + (f_\beta + f_\gamma) X}{f_\alpha + (f_\beta + f_\gamma)} = \frac{f_\alpha C_\alpha + f_\beta C_\beta + f_\gamma C_\gamma}{f_\alpha + f_\beta + f_\gamma}$, that is, the homogeneous barycentric coordinate of the theoretical fractions plotted on the axes of triangle $\alpha\beta\gamma$, where each of them corresponds to the two-component mixing among the endmembers plotted at side's ends. The following results will practically test this approach.

4 | RESULTS

4.1 | Hydraulic relationship between the Riardo Plain and Mt. Maggiore aquifers

Monitoring wells *N* and *F* (location in Figure 1) show similar groundwater levels, both instantaneously and over 563 days of monitoring throughout the study (the experimental data are showed in the Figure 3), indicating that the aquifers are hydraulically connected and nearly continuous across both the volcanic deposits and the carbonate basement. *F* is the only monitoring well that taps the phreatic carbonate aquifer of Mt. Maggiore. The saturation level in this well is ~ 1.5 m higher than the recorded one in *N* well.

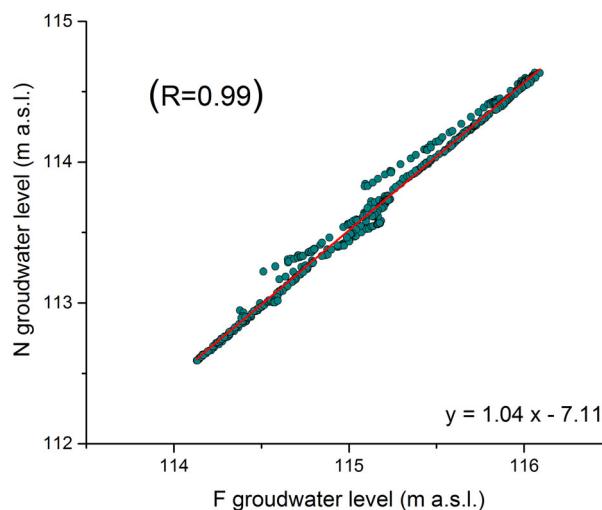


FIGURE 3 Linear correlation between mean daily groundwater level data measured in *F* and *N* monitoring wells

The groundwater oscillations are in agreement with the local climatic conditions and therefore with the recharge for the region as reported in Viaroli et al. (2018). The strict linear correlation ($R = 0.99$, $p < 0.001$) between the mean daily groundwater level data (Figure 3) demonstrates the hydraulic connection between the aquifers of Mt. Maggiore and the Riardo Plain. The oscillations of the groundwater level are simultaneous, with a very similar magnitude.

4.2 | Determination of the suitable tracers

The whole dataset of chemical analysis is reported in the dataset stored in the specific repository (Cuoco, Viaroli, Darrah, et al., 2021), while a data summary for all monitored wells is shown in Table 1. In the dataset, each monthly sampling point has been identified with a lower-case letter of Latin alphabet.

The suitability of each chemical variable is evaluated to determine its effectiveness as a potential tracer. The chemical variables involved in the fraction computations for each tracer must respect important constraints in order to get a reliable mixing model (Elsenbeer et al., 1995; Inamdar, 2011; Liu et al., 2017)

These constraints include:

1. The tracers in the mixing process must exhibit a linear relationship;
2. The tracers must behave conservatively in aqueous solutions;
3. The components have significantly different concentrations for at least one tracer;
4. The concentrations of each tracer in each endmember must be consistent throughout the investigated area or over the time scale considered for the mixing model.

The mixing process related to the dilution of the more concentrated endmember produces linear correlations among water solutes (Hooper, 2003). In the correlation matrix, reported in the dataset

TABLE 1 Summary of the whole dataset presented in the stored dataset Cuoco, Viaroli, Darrah, et al. (2021)

	T (°C)	pH	EC (µS/cm)	ORP (mV)	HCO ₃ ⁻ (mg/L)	F (mg/L)	Cl (mg/L)	NO ₃ ⁻ (mg/L)	SO ₄ ⁻² (mg/L)	Na (mg/L)	K (mg/L)	Mg (mg/L)	Ca (mg/L)	Li (µg/L)	B (µg/L)	V (µg/L)	Mn (µg/L)	Fe (µg/L)	As (µg/L)	Rb (µg/L)	Sr (µg/L)	Cs (µg/L)	Ba (µg/L)	SI CaCO ₃	SI CaMg(CO ₃) ₂	
#26	Mean	15.8	6.13	2378	99	1761.6	0.8	19.7	2.8	59.0	56.7	45.8	440.3	109	660	6	225	390	6	110	912	47	130	0.22	-0.30	
	Min	15.0	5.93	2250	51	1684.6	0.6	17.3	2.2	50.3	44.8	35.4	406.0	101	621	6	87	205	5	97	867	37	120	0.07	-0.73	
	Max	16.5	6.28	2500	126	1981.0	1.1	22.9	3.5	3.3	66.0	65.8	497.3	122	763	7	342	605	8	125	961	51	141	0.37	0.02	
	RSD	2.9	1.7	3.1	23.1	4.8	19.9	8.1	44.1	12.4	8.2	10.4	14.4	6.1	4.9	5.8	7.4	42.6	34.7	18.3	5.6	3.1	10.0	4.8		
	%																									
#20	Mean	16.3	5.94	1785	138	1181.6	0.8	19.3	2.7	50.8	44.0	26.8	297.0	62	440	10	7	5	10	137	640	6	49	-0.26	-1.33	
	Min	15.7	5.80	1621	101	1098.4	0.7	16.7	2.1	42.8	31.7	18.3	258.9	54	383	9	3	2	9	121	584	5	44	-0.41	-1.66	
	Max	17.5	6.09	2722	227	1345.1	1.0	23.6	10.9	3.4	64.9	58.4	32.5	340.9	71	494	11	8	10	11	150	701	7	55	-0.10	-0.98
	RSD	3.0	1.4	14.8	22.8	4.9	12.0	9.7	16.9	16.0	14.5	16.8	14.9	7.3	8.7	9.8	7.2	23.1	35.4	-	6.9	5.3	8.8	6.5		
	%																									
#16	Mean	15.3	6.03	1715	124	1181.3	1.0	18.1	4.9	60.7	48.9	28.6	285.1	81	252	8	221	91	11	179	631	5	27	-0.21	-1.21	
	Min	14.5	5.90	1678	93	1118.7	0.8	15.9	2.9	4.1	52.4	42.1	22.6	250.3	76	235	7	115	64	10	162	586	4	22	-0.36	-1.59
	Max	16.4	6.18	1756	182	1366.8	1.2	21.1	9.2	5.8	66.4	55.0	34.0	323.8	87	276	8	252	104	11	197	672	6	56	-0.11	-0.93
	RSD	3.4	1.2	1.2	20.8	5.5	9.6	7.6	23.4	8.8	7.1	7.8	13.7	6.2	4.9	5.4	4.2	15.7	10.9	3.1	6.2	4.4	10.2	31.1		
	%																									
#17	Mean	15.7	5.99	1313	124	854.1	0.6	19.2	6.2	36.2	27.1	21.6	226.3	61	243	7	192	5	6	169	693	15	43	-0.43	-1.66	
	Min	15.0	5.87	1260	76	776.5	0.5	16.8	15.7	5.5	31.4	23.4	16.9	206.5	58	207	7	52	0.4	6	141	590	11	34	-0.58	-2.07
	Max	16.4	6.12	1452	169	937.0	0.8	22.6	20.4	7.1	41.2	32.8	25.2	247.2	65	316	9	260	10	7	200	686	20	64	-0.34	-1.47
	RSD	2.5	1.1	4.2	20.0	5.3	21.4	8.8	9.0	7.1	8.6	11.2	11.5	4.8	3.8	12.6	7.2	26.1	58.0	6.6	9.5	4.9	22.7	18.9		
	%																									
#27	Mean	16.5	6.32	3211	8	2550.2	0.7	21.9	1.9	77.6	65.3	61.7	640.1	142	702	2	627	4455	11	184	1429	9	242	0.63	0.35	
	Min	16.0	6.26	2980	-30	2403.6	0.4	19.3	bdl	1.4	70.6	55.1	45.1	569.1	109	603	1	461	2167	8	172	1375	7	227	-0.34	-1.47
	Max	17.4	6.41	3270	34	3432.4	1.0	24.8	bdl	2.4	84.3	71.1	78.5	854.4	163	792	2	679	5542	11	203	1552	10	257	0.72	0.71
	RSD	2.8	0.7	2.2	276.9	10.1	24.8	8.8	-	14.7	5.7	7.1	14.6	10.4	12.0	7.4	14.1	8.2	16.3	10	5.1	3.1	8.3	3.2		
	%																									
#25	Mean	17.1	6.12	2114	59	1501.1	1.3	17.5	bdl	54.0	58.2	31.9	387.5	98	590	3	360	2247	13	118	914	58	167	0.11	-0.62	
	Min	15.8	6.01	1795	22	1281.4	0.9	14.3	bdl	2.1	41.3	49.0	22.8	325.4	73	416	3	267	1338	9	98	673	43	121	0.00	-0.96
	Max	18.6	6.22	2290	90	1708.6	1.5	20.0	bdl	3.7	65.5	69.1	39.4	425.5	111	639	3	395	2805	17	136	1009	70	216	0.25	-0.30
	RSD	5.3	1.3	6.4	36.7	8.2	14.1	9.2	-	14.9	14.6	10.7	16.0	6.5	11.3	10.5	9.7	10.2	19.1	21	8.6	10.2	15.8	17.1		
	%																									
N	Mean	14.9	6.41	431	109	218.1	1.1	15.1	6.5	30.9	27.9	6.7	33.0	31	92	15	1	2	9	70	110	9	14	-1.31	-3.09	
	Min	14.2	6.31	415	84	203.4	1.0	12.7	4.3	3.0	27.4	24.3	6.0	30.1	29	86	14	1	1	62	101	8	12	-1.43	-3.39	
	Max	16.3	6.57	449	143	231.9	1.2	16.4	7.7	4.3	34.3	30.8	7.6	36.2	31	95	16	1	5	80	114	10	16	-1.12	-2.72	
	RSD	4.1	1.2	2.7	19.3	3.8	8.7	7.6	16.4	9.8	6.7	6.8	8.6	6.2	2.3	2.9	4.2	15.7	54.4	1.6	7.5	3.2	6.9	8.6		
	%																									
F	Mean	15.3	7.67	434	73	243.1	0.3	18.1	0.7	9.5	11.8	3.1	20.5	55.8	4	14	2	bdl	4	1	18	114	1	10	0.21	0.19
	Min	13.8	7.43	421	32	221.9	0.1	17.5	0.2	8.5	10.3	2.5	17.6	49.6	3	11	2	bdl	1	1	16	105	1	8	0.04	-0.12
	Max	17.6	7.83	459	119	268.5	0.5	19.4	1.0	11.4	13.5	3.8	22.7	62.3	6	17	2	bdl	7	1	21	127	2	13	0.35	0.44
	RSD	9.3	1.7	3.1	32.6	6.5	75.1	3.4	41.2	9.1	8.0	14.5	8.8	7.7	21.9	11.6	6.7	-	45.3	15.7	9.7	6.5	51.5	14.6		
	%																									
D	Mean	16.8	6.2	3367	-34.8	2606.7	1.4	24.1	1.1	84.0	86.4	54.0	665.0	154	1095	0.2	652	5810	35	169	1721	78	281	0.54	0.24	
	Min	16.5	6.2	3296	-42.0	2481.5	1.1	23.0	bdl	0.7	81.7	84.1	49.8	655.6	89	815	0.2	596	3895	21	157	1511	39	197	0.50	0.12
	Max	17.3	6.2	3490	-25.0	2683.3	1.7	24.7	bdl	1.7	88.3	88.6	57.8	675.7	202	1381	0.2	780	8084	46	176	1845	120	335	0.59	0.36
	RSD	1.9	0.6	2.7	-17.9	3.3	15.5	2.7	-	37.1	2.9	2.2	5.4	1.0	31.9	18.3	-	10.9	27.7	31.1	4.8	6.8	41.4	17.9		
	%																									

Note: D, N and F are the endmembers, the other groundwater wells have the same ID as presented in Cuoco et al. (2020). Abbreviations: nd, not detected; RSD, relative SD.

(Cuoco, Viaroli, Darrah, et al., 2021), most of the chemical variables are well correlated, indicative of mixing, as demonstrated by Cuoco et al. (2020). This statistical relationship is shown in Figure 4a,b where the EC versus HCO_3^- (Figure 4a) and Na^+ versus K^+ (Figure 4b) display highly significant correlations ($R^2 = 0.99$ and 0.95 respectively, $p < 0.001$). Similar linear correlations ($R \approx 0.90$) have been found among the most of highly mobile elements: alkali elements with exception of Rb and Cs, alkali earth elements, HCO_3^- , B and EC.

In order to behave conservatively, a variable must not be affected by any chemical reaction. In the investigated system the chemical reactions which can occur are: (i) the re-equilibration of water solution with the CO_2 degassing; (ii) redox re-equilibration due to the mixing between the low ORP deep water and the more oxidant one in the shallow aquifer; (iii) hydrolysis of minerals/volcanic glass and (iv) ion adsorption on the host rock and on chemical precipitates.

According to calculations performed using PHREEQC (Parkhurst & Appelo, 1999), waters with EC $> 2000 \mu\text{S/cm}$ are saturated (saturation index, SI > 0) with respect calcite and those with EC $> 2500 \mu\text{S/cm}$ are saturated with respect dolomite (see Table 1). Thus, even though samples from monitoring well F are less mineralized (EC $\sim 400 \mu\text{S/cm}$), they were saturated with respect to calcite and dolomite as a result of influences from the Mt. Maggiore carbonate aquifer (Mazza et al., 2013).

The Ca, Mg and HCO_3^- concentrations in solution of the resulting mixture depend on the precipitation equilibria of calcite and dolomite related to the ionic strength of the solution and the CO_2 concentration (Drever, 1997; Kehew, 2001; Langmuir, 1997). As a free gas, carbon dioxide migrates in the water column differently than when dissolved in solution and therefore, the chemical equilibrium is not exclusively related to mixing processes of distinct water parcels. Because of this lack of conservative behaviour, Ca, Mg, HCO_3^- and pH (i.e., $[\text{H}^+]$) are thus not considered suitable tracers. EC is strongly correlated to these solutes (Cuoco, Viaroli, Darrah, et al., 2021), and thus is also dismissed as unreliable because of its non-conservative behaviour.

The dissolved oxygen concentration is the main geochemical variable that influences ORP (Stumm & Morgan, 1996). When oxygen levels increase after mixing, Fe and Mn-rich form nearly insoluble oxyhydroxides and precipitate on the surfaces of aquifer minerals (Ahmad et al., 2019); this process is observed in D samples. Here, we observe an inverse correlation ($R = -0.83$) between Fe and Mn relative to ORP (Cuoco, Viaroli, Darrah, et al., 2021) indicating that both species are likely lost to precipitation after oxidation, as would be expected. Some tracers, including Ba, Sr and As ($R \sim 0.9$), also correlate strongly with Mn and Fe. These trends suggest that these elements are also likely absorbed onto or co-precipitate with Fe/Mn precipitates (Dowling et al., 2002; Rashad et al., 2008) as we previously suggested in this region (Cuoco et al., 2020) and as it has recently investigated in depth (Cuoco, Viaroli, Paolucci, et al., 2021). Thus, we also conclude that neither Fe nor Mn (or even Ba, Sr or As) are effective tracers for the mass balance computations because of their redox sensitive behaviour. For a similar reason SO_4^{2-} has been discarded as tracer because it can be produced by oxidation of H_2S present in the gas emissions. The lack of accurate quantifications of the chemical species involved in the $\text{H}_2\text{S}-\text{H}_2\text{O}-\text{O}_2-\text{SO}_4^{2-}$ system force us to not trust on sulphate as conservative element. Vanadium is also redox sensitive but is mobile in oxidizing conditions (Coyte & Vengosh, 2020). The ORP changes due to the mixing between the shallow oxidant groundwater with the deep and anoxic groundwater, however during this process the solution does not attain negative values required for V reduction (Shaheen et al., 2019). Thus, the variation of V concentrations are only related to the dilution, and therefore it can be considered as conservative tracer in these conditions.

Ion exchange processes may also affect the chemical composition of water solutions (Appelo & Postma, 2005). When groundwater flows into volcanic successions, it is exposed to exchange sites present on the rocks and on Fe and Mn precipitates. The $(\text{Na} + \text{K})/(\text{Mg} + \text{Ca})$ is commonly used to determine if the adsorption-desorption reactions have altered the chemical composition of the major ions. If the exchange reactions did not affect the composition of dissolved

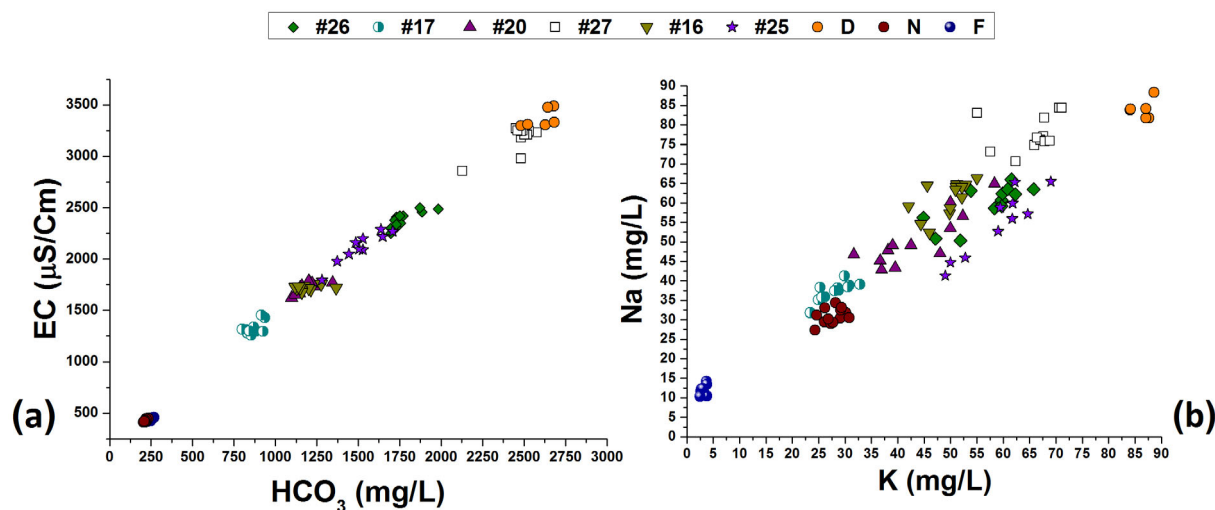


FIGURE 4 Linear relationship between HCO_3^- versus EC (a), and K versus Na (b) as consequence groundwater mixing among endmembers with different in ionic concentrations and CO_2 abundances

ions, the ratio in the mixing dynamics would be constant, and therefore the metals concentrations exclusively depending on the dilution effect.

In the *D* samples, the mill-equivalents ratio $(\text{Na} + \text{K})/(\text{Mg} + \text{Ca})$ was approximately equal to 0.1–0.2 (the linear correlation of $\text{Na} + \text{K}$ versus $\text{Ca} + \text{Mg}$ displayed $R^2 = 0.78$, suggesting a quite constant angular coefficient, i.e., ratio value) and remained nearly constant throughout the sample set with the exception of samples from unmixed *N* endmember (0.9–1.0), which reflects the specific ratio of the shallow volcanic aquifer. Therefore, the major alkali ions Na and K are apparently not strongly affected by ion exchange dynamics and can be considered effective as tracers for mixing fraction quantification.

Conversely, trace alkali and alkali earth metals were not considered reliable tracers because their concentrations are 1000 times less concentrated than major ions and thus the effect of interactions with exchange sites may more readily affect their concentration in solution. Other trace elements such as Li, B, Ba, Cs were not constant in the *D* aquifer during the monitoring period. The relative SD (RSD) of major elements (Table 1) were all less than 5%, while the trace elements differed by between 10% and 50%. Thus, we would not consider trace elements, with the exception of V, when constructing mixing models.

The last step in the selection of suitable tracers is an evaluation of significant differences in the endmember's concentrations. This decision-making process can be led by observing the statistical distribution of the chemical variables in the dataset. If the concentration of a tracer is similar in all the endmembers, the solution produced by the

mixing will not have a significantly different concentration. As a result, tracer behaviour will mimic a random variable and likely display a similar statistical distribution to a normal frequency function. Figure 5 shows the histograms of Na, K, V and Cl concentrations. Note that Cl, which is widely considered as one of the best tracers for mass balances in water mixing due to its highly conservative behaviour in solution (Harkness et al., 2017; Hendry et al., 2000; Warner et al., 2012), follows a normal distribution (Shapiro–Wilk test, $p = 0.071$); thus, we conclude that Cl is not a suitable tracer in this current study area. Similarly, temperature, pH and *F* are also normally distributed and not suitable tracers ($p > 0.054$).

Conversely, Na and K have a larger concentration range (0–90 mg/L vs. 12–26 mg/L respectively, Figure 5) than Cl (and their frequency distribution is not normally distributed, Shapiro–Wilk test, $p < 0.006$). Similarly, the concentration of V varies by nearly two orders of magnitude (0.1–18 $\mu\text{g/L}$) and is also not normally distributed (Shapiro–Wilk test, $p < 0.001$). As a result, these tracers pass the test of suitable tracers for mixing calculations in the current study area.

4.3 | Characterization of endmembers and related tracers

We consider three endmembers, based on data from the *D*, *N* and *F* sample subsets. *D* samples were collected through boreholes tapping the carbonate aquifer under the Riardo Plain. The *D* groundwater

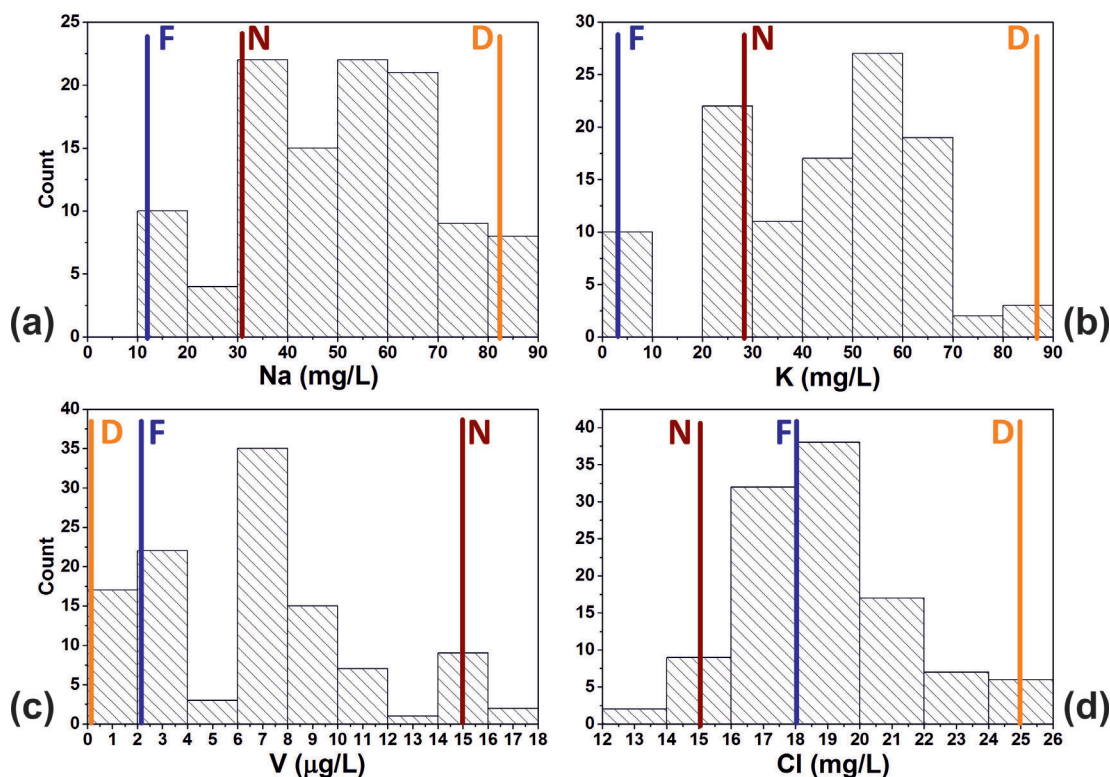


FIGURE 5 Histograms of detected concentrations of Na (a), K (b), V (c) and Cl (d). Cl is normally distributed while Na, K and V follow a multimodal distribution. Orange, blue and maroon bars correspond to the mean concentration in *D*, *F* and *N* samples, respectively

subset has the highest mineralization detected in the area ($\sim 3000 \mu\text{S}/\text{cm}$), the lowest ORP (-35 mV), and the highest CO_2 content ($0.05 \text{ mol}/\text{kg}$, PHREEQC computer code). Each of these factors strongly enhance carbonate hydrolysis with important increases in Ca and HCO_3 in solution and a positive calcite saturation index ($\text{SI}_{\text{CaCO}_3} \sim 0.6$).

The *N* endmember corresponds to the groundwater hosted in the volcanic deposits and it is characterized by low mineralization ($\sim 430 \mu\text{S}/\text{cm}$), the highest ORP (110 mV) observed in this study and low CO_2 concentrations ($0.004 \text{ mol}/\text{kg}$). We anticipate that the mixing process occurred where more deeply sourced fluids migrated along the fault planes as depicted by the linear relationship (Figure 4) between the mineralization level (EC) and HCO_3 (and indirectly also the CO_2 levels in solution) (Drever, 1997). The linear function is due to mixing, but when one only considers the variables in the binary plots of Figure 4, the third endmember (*F*) is not distinguished from the *N* endmember.

The *F* endmember corresponds to the Ca–Mg– HCO_3 type groundwater water, hosted in the carbonate units of the Mt. Maggiore and in hydraulic continuity with the aquifer of the plain. The mineralization level of endmember *F* and the CO_2 concentrations are similar to those of *N*. Based on prior interpretations for three-component mixing, we attempt to determine which chemical variables distinguish the differences between the three endmembers.

The *D* endmember is dominated by Ca– HCO_3 , but shows the highest concentrations of major ions, alkali and alkaline earth elements and trace elements due to water–rock interactions with the Roccamonfina volcano deposits (Cuoco et al., 2010, 2020; Viaroli et al., 2018). *N* is a Na–K– HCO_3 type water, typical of groundwater in volcanic aquifers from central Italy (Gambardella et al., 2005). All trace elements (e.g., metals, with the exception of vanadium) derived from leaching of the volcanic deposits are more concentrated in *D* than in *N*. Vanadium is more concentrated in the *N* ($15 \mu\text{g}/\text{L}$) than in *D*, where concentrations near the detection limit ($\sim 0.2 \mu\text{g}/\text{L}$) have been observed.

In the carbonate endmember *F*, all the trace metals and metalloids have the lowest concentrations except V, which is consistently near $2 \mu\text{g}/\text{L}$. In cross plots of K versus V (Figure 6a), the components *D*, *N* and *F* plot at the vertices of a ternary diagram, reproducing the theoretical condition displayed in the Figure 2b. The water solutions produced by the mixing of these three endmembers plot inside the area of the triangle. The detected configuration does not change if K is replaced with Na.

4.4 | Fractions quantification and analytical representation

After the selection of K, Na and V as tracers, the mixing fractions have been computed using the algebraic solution of the mass balance equations (Liu et al., 2017; Ogunkoya & Jenkins, 1993). For a three-component mixture, two tracers are necessary in the calculation. The uncertainties have been computed by Gaussian error propagation (Genereux, 1998). The full results are reported in stored dataset

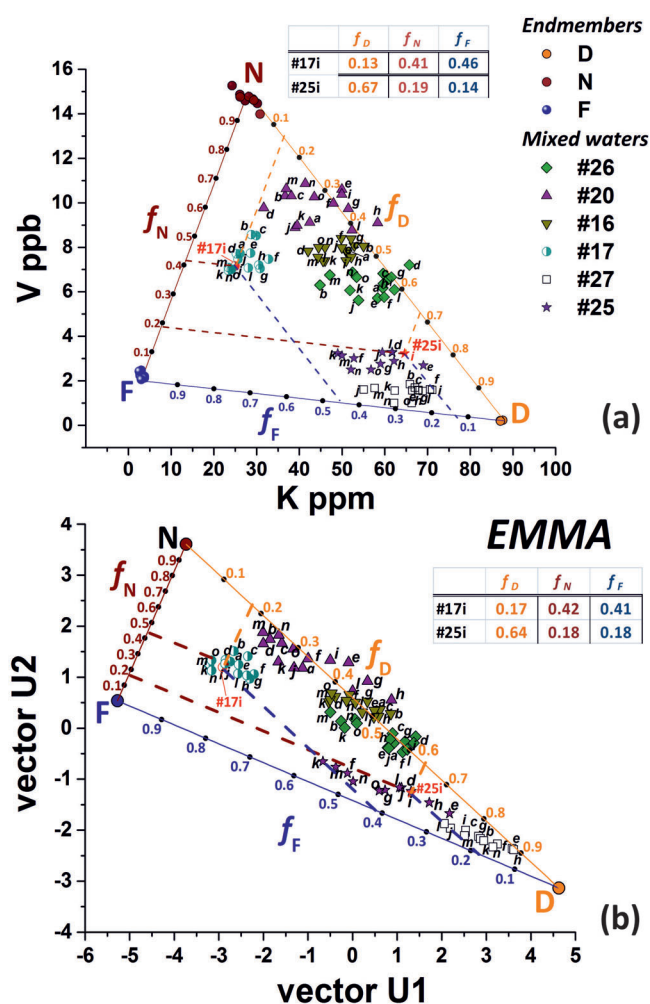


FIGURE 6 Three-component mixing represented by a bidimensional space defined by (a) element–element cross plots of K versus V and (b) End member mixing analysis (EMMA) results. Each single sample point is detected by the letter used as sub-ID and reported in the Cuoco, Viaroli, Darrah, et al. (2021). The mixing fractions detected by homogenous barycentric coordinates correspond to the ones computed with equations

(Cuoco, Viaroli, Darrah, et al., 2021) and summarized the Table 2. The mixing fractions have been obtained both by cross plots of Na versus V and K versus V, whereas the cross plots of Na versus K have not been considered due to the similarity in concentrations between the endmembers (Table 1).

The variability of the calculated fractions was evaluated through Mann–Whitney rank sum tests ($\alpha = 0.05$) and were not statistically significant different ($p > 0.091$) suggesting that the quantifications obtained through Na–V and K–V couples gave similar mixing estimates. In the Figure 6a, the mixing lines between various endmembers have been calculated according to Equations (11)–(13). The theoretical fractions with an increment of 0.1 have been reported on all mixing lines. Note the close relationship between the calculated mixing fractions computed by algebraic solutions (reported in Cuoco, Viaroli, Darrah, et al., 2021) with the geometrical solutions following the barycentric coordinates method (Figure 6). Based on these computations, we can calculate the fraction of each individual groundwater

TABLE 2 Summary of mixing fractions quantifications

	fD		±ΔfD		fD		±ΔfD		fN		±ΔfN		fN		±ΔfN		fF		±ΔfF		fF		±ΔfF		
	K-V	Na-V	K-V	Na-V	K-V	Na-V	K-V	Na-V	K-V	Na-V	K-V	Na-V	K-V	Na-V	K-V	Na-V	K-V	Na-V	K-V	Na-V	K-V	Na-V	K-V	Na-V	
#26	Min	0.37	0.41	0.03	0.42	0.42	0.06	0.06	0.35	0.04	0.36	0.04	0.36	0.04	0.36	0.01	0.01	-0.08	0.04	-0.08	0.04	-0.02	0.04	-0.09	0.05
	Max	0.60	0.58	0.05	0.60	0.60	0.07	0.07	0.48	0.06	0.48	0.07	0.49	0.07	0.49	0.02	0.02	0.24	0.06	0.24	0.06	0.21	0.06	0.17	0.08
	Mean	0.51	0.51	0.04	0.53	0.53	0.06	0.06	0.41	0.05	0.41	0.05	0.41	0.05	0.41	0.01	0.01	0.08	0.05	0.08	0.05	0.08	0.05	0.05	0.07
#20	Min	0.15	0.23	0.03	0.22	0.22	0.07	0.07	0.56	0.07	0.58	0.06	0.58	0.06	0.58	0.02	0.02	-0.08	0.05	-0.08	0.05	-0.16	0.05	-0.15	0.07
	Max	0.47	0.52	0.04	0.52	0.52	0.09	0.09	0.71	0.08	0.72	0.08	0.63	0.08	0.63	0.02	0.02	0.23	0.06	0.23	0.06	0.15	0.06	0.15	0.09
	Mean	0.29	0.34	0.04	0.33	0.33	0.08	0.08	0.64	0.07	0.65	0.07	0.66	0.07	0.66	0.02	0.02	0.07	0.06	0.07	0.06	0.01	0.06	0.01	0.08
#16	Min	0.31	0.41	0.03	0.40	0.40	0.06	0.06	0.46	0.05	0.47	0.05	0.48	0.05	0.48	0.01	0.01	0.02	0.05	0.02	0.05	-0.10	0.05	-0.09	0.06
	Max	0.46	0.56	0.04	0.53	0.53	0.07	0.07	0.55	0.06	0.56	0.06	0.57	0.06	0.57	0.02	0.02	0.20	0.05	0.20	0.05	0.11	0.06	0.12	0.08
	Mean	0.39	0.50	0.03	0.46	0.46	0.07	0.07	0.50	0.06	0.52	0.06	0.53	0.06	0.53	0.02	0.02	0.11	0.05	0.11	0.05	-0.01	0.05	0.01	0.07
#17	Min	0.11	0.19	0.02	0.14	0.14	0.06	0.06	0.38	0.05	0.39	0.05	0.38	0.05	0.38	0.02	0.02	0.32	0.04	0.32	0.04	0.20	0.04	0.25	0.07
	Max	0.21	0.27	0.03	0.24	0.24	0.07	0.07	0.53	0.06	0.54	0.06	0.54	0.06	0.54	0.02	0.02	0.50	0.05	0.50	0.05	0.42	0.05	0.47	0.08
	Mean	0.15	0.23	0.03	0.19	0.19	0.06	0.06	0.44	0.06	0.45	0.06	0.35	0.06	0.35	0.02	0.02	0.41	0.04	0.41	0.04	0.32	0.04	0.37	0.08
#27	Min	0.59	0.75	0.03	0.73	0.73	0.08	0.08	0.02	0.01	0.04	0.01	0.04	0.01	0.04	0.02	0.02	0.15	0.03	0.15	0.03	0.00	0.04	0.02	0.08
	Max	0.78	0.90	0.04	0.88	0.88	0.10	0.10	0.09	0.01	0.10	0.01	0.11	0.03	0.11	0.03	0.03	0.36	0.04	0.36	0.04	0.02	0.05	0.19	0.11
	Mean	0.71	0.83	0.04	0.81	0.81	0.09	0.09	0.06	0.01	0.08	0.01	0.09	0.02	0.09	0.02	0.02	0.23	0.03	0.23	0.03	0.09	0.04	0.11	0.10
#25	Min	0.49	0.38	0.02	0.44	0.44	0.05	0.05	0.12	0.02	0.11	0.02	0.10	0.02	0.10	0.01	0.01	0.12	0.03	0.12	0.03	0.18	0.03	0.12	0.06
	Max	0.73	0.67	0.04	0.73	0.73	0.08	0.08	0.19	0.02	0.18	0.02	0.18	0.02	0.18	0.02	0.02	0.35	0.04	0.35	0.04	0.47	0.04	0.41	0.08
	Mean	0.60	0.53	0.03	0.58	0.58	0.06	0.06	0.16	0.02	0.15	0.02	0.15	0.02	0.15	0.02	0.02	0.24	0.04	0.24	0.04	0.32	0.03	0.27	0.06

Note: The fractions of each endmember with related uncertainty computed with mass balances (K-V and Na-V couple of tracers), and EMMA method are reported. The detailed dataset is reported in Cuoco, Viaroli, Darrah, et al. (2021).

sample with respect to the coordinates of the three endmembers (f_D , f_F and f_N). Two examples (#17i and #25i) are reported on Figure 6a, which can be used to describe the relative contributions to each water sample. The closeness with D vertex detected in samples #25 and #27 indicate the high fractions of the deep D endmember observed in these samples. These two wells show an almost stable N fraction (#25 \approx 0.20; #27 $<$ 0.10) and an inverse mutual relation between the D (#25 0.40–0.70; #27 0.60–0.80) and F (#25 0.10–0.45; #27 0.10–0.30) fractions during the monitoring period. The highest F fractions have been detected in #17 well (0.20–0.50, Figure 6a). Wells #26, #16 and #20 display negligible F fractions (values consistent with the zero), consequently the sample points plot close the D – N axis; these results suggest that the composition of the last three wells are dominantly two-component mixing with only minor F fraction oscillations (up to 0.20).

The EMMA is a mathematical method based on multivariate statistics, used to identify and quantify the endmembers contribution in complex hydrological systems (Christophersen et al., 1990; Christophersen & Hooper, 1992; Hooper et al., 1990). EMMA methods are applied to the whole dataset without any previous supposition about the endmembers. It is only necessary to choose the effective tracers, which will subsequently be tested as part of the procedure (Hooper, 2003). Here, we tested the EMMA method using the same three geochemical tracers (i.e., Na, K, V).

The principal components have been extracted after the data normalization (Joreskog et al., 1976). The number of endmembers is given by $m + 1$, where m is the number of eigenvalues retained. In the present study only two principal components ($m = 2$) were extracted, explaining respectively the 78% and the 18% of total variance. The first principal component describes the relative abundance of alkali ions, while the second principal component appears to vary with changing V concentrations. The presence of three endmembers is thus confirmed by the EMMA outcomes suggesting that the proposed mixing model robustly captures each endmember.

The product of our chosen geochemical tracer matrix with the transposition of eigenvectors matrix give a new U space where endmembers and mixed solutions are projected, in other words U is a lower dimensional mixing subspace. Being the data matrix $n \times 3$ (where n is the number of samples) and $3 \times m$ (in the present investigation $m = 2$), the U space is therefore the transformed data matrix ($n \times m$). For a three-component mixture, the U space results are bidimensional (Figure 6b) and the sample data are projected onto the U space. The three endmembers are confirmed to be D , N and F , which correspond to the vertexes of the ternary diagram Figure 6a. Based on Equations from (8) to (13), once fixed at theoretical fractions, the concentrations of Na, K and V are computed. These 'theoretical' concentrations are added to data input in the EMMA elaboration. The theoretical fractions, with the obtained new coordinates in the U space in the Figure 6b plot on the axes of the resulting reference triangle.

Following Osemwegie et al. (2018) the theoretical endmembers can be defined as such:

$$U_{1p} = f_D U_{1D} + f_N U_{1N} + f_F U_{1F} \quad (15)$$

$$U_{2p} = f_D U_{2D} + f_N U_{2N} + f_F U_{2F} \quad (16)$$

$$f_D + f_N + f_F = 1 \quad (17)$$

where U_1 and U_2 are the two vectors defining the mixing subspace U , U_{1p} and U_{2p} are the coordinates of p (generic sample point whose chemical composition is the produced by the three-component mixing) and D , N and F subscripts detects the coordinates of the three endmembers. Combining Equations (15)–(17), the mixing fractions can be obtained as follows:

$$f_D = \frac{[U_{2p}(U_{1N} - U_{1F})] - [U_{1p}(U_{2N} - U_{2F})] + [U_{1F}(U_{2N} - U_{2F})] - [U_{2F}(U_{1N} - U_{1F})]}{[(U_{2D} - U_{2F})(U_{1N} - U_{1F}) - (U_{1D} - U_{1F})(U_{2N} - U_{2F})]} \quad (18)$$

$$f_N = \frac{[U_{1p} - f_D(U_{1D} - U_{1F})] - U_{1F}}{(U_{1N} - U_{1F})} \quad (19)$$

$$f_F = 1 - (f_D + f_N) \quad (20)$$

Mixing fractions computed through the EMMA method have been reported in Cuoco, Viaroli, Darrah, et al. (2021) and summarized in the Table 2. The uncertainties were computed according to Burns et al. (2001) and resulted in the same order of magnitude of the simple algebraic mixing fractions computing. Like Figure 6a, the computed fractions of each point are detected by the barycentric coordinate system using theoretical fractions reported on the sides of the triangle. In the Figure 6b, the computed fractions of the same points evidenced in the Figure 6a have been reported with the aim to show the correspondence of values obtained by both algebraic and geometrical methods.

Comparing the results of algebraic and EMMA method, the calculated endmembers fractions and uncertainties gave similar results. The mixing fractions computed with algebraic equations ($\Delta f_{\text{algebraic}}$) and EMMA (Δf_{EMMA}) methods have been compared in Figure 7a–c. The strong convergence of obtained results with the two different methods is confirmed by statistically significant determination factors of the best fit ($R^2 > 0.89$, $p < 0.001$) and the parameters of the fit line (the angular coefficient equal to 1 and intercept near zero). The differences are quantified as $\Delta f = \sqrt{(f_{\text{algebraic}} - f_{\text{EMMA}})^2}$ and the results are summarized in the Figure 7d using box plots. The totality of Δf_N quantifications are below 0.05, while the 75% of the other fractions are below 0.10. Only the 14% of Δf_F values range between 0.10 and 0.15.

5 | DISCUSSION

5.1 | The ternary diagram as a tool for quantification and comparison of three component mixing processes

The present investigation allowed us to test variable mixing models for fast computation and presentation of results in three-component

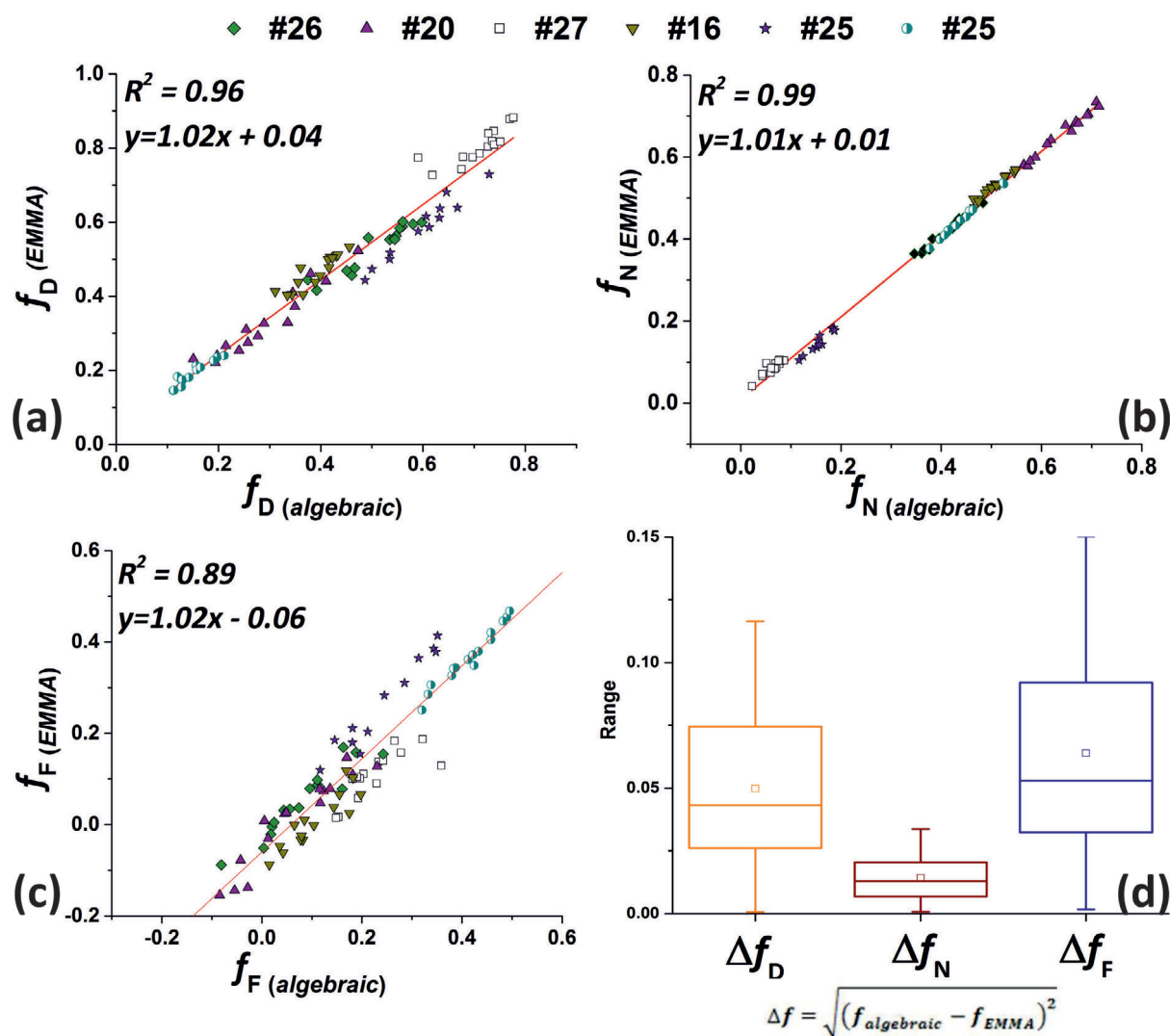


FIGURE 7 Comparison of quantifications of three mixing fractions: f_1 (a), f_2 (b) and f_3 (c) obtained through mass balance algebraic equations and end member mixing analysis (EMMA) method. (d) Box plots for the three fractions distance Δf computed through the showed formula

mixing. The bidimensional space representing the water mixing (Figure 6) has been built following the theoretical considerations presented in Section 3.3. The triangle defined by the three endmembers act as a reference for a homogeneous barycentric coordinates system. Once the theoretical fractions are reported on the sides of triangle, the mixing fractions can be obtained through this geometrical method. With respect the algebraic computation of mixing fractions, this method allows a rapid evaluation of the endmember's fractions in each sample, and in addition this graphical method also has the advantage of allowing for easy comparison between various mixing fractions of the different analysed waters. This method is suitable both for small or large datasets. The main advantage is the fast comparison of endmembers' fractions of each sample. A weakness of this method is the resolution of the computed results when a thickened dataset is used. Every type of graphical representation is affected by this problem, but in this case it is even possible to get a rough idea of endmembers' percentages according to the points' positions on the

graph. The potential of the proposed approach was not highlighted elsewhere before.

This graphical method works both in the algebraic computations considering a binary tracer-tracer plot and in EMMA elaboration by projecting the theoretical fractions in the bidimensional space detected by the three endmembers, as it must result in a three-component mixing. The good agreement of results in the present investigation confirms that projection of the theoretical fractions on the mixing subspace detected in the EMMA method allow reliable quantitative evaluations, if the model assumptions are correct.

5.2 | Elements to evaluate a chemical variable as tracer in a hydrogeochemical dataset

The strong correlations among water solutes in mixing dynamics, as detected by Cuoco et al. (2020) in the study area, do not necessarily

serve as a reliable index for evaluating mixing. In fact, herein we note that when evaluating the three-component mixing, the correlation decreases when any of chemical variables have relevant concentrations in all three endmembers simultaneously. For example, when V is compared to Na or K , the Pearson's coefficient (R) decreases (~ -0.2 , see Cuoco, Viaroli, Darrah, et al., 2021). While the Pearson's R coefficient could be a good index for two-component mixing, it does not necessarily indicate conservative behaviour of the specified geochemical tracers. One or both variables can be affected by other chemical reactions or the same reaction (e.g., Ba and Sr adsorption onto iron oxyhydroxides).

Another issue which cannot be neglected for a correct mixing model assessment, is the statistical distribution in the dataset of the tracers. Szulczewski and Jakubowski (2018) observed that a dataset produced by mixing follows a multimodal distribution, as it is confirmed in the Figure 5 for the Na , K and V histograms. Cl , which is usually assessed as a powerful tracers due to its conservative behaviour, in the study system shows a normal distribution and consequently the fractions computed using Cl , both using the simple algebraic and EMMA method are not reliable. The fact that a geochemical tracer must have different concentrations at least in one of the endmembers means that a geochemical tracer cannot follow a single mode distribution in the dataset. Moreover, if it does follow a single mode distribution, it indicates that the considered variable does not act as an effective geochemical tracer in that study area.

5.3 | New experimental evidences on the hydrological processes governing the FGS

The hydrogeological setting of the FGS make it an ideal site to examine the processes of three-component mixing in groundwater. The synchronous fluctuations of groundwater levels across the region indicate clear evidence of hydraulic communication between Mt. Maggiore and the Riardo Plain aquifers (Figure 1), which was inferred by Cuoco et al. (2020) based on exclusively geochemical data. Based on the numerical methods of distinguishing between various groundwater contributions, we can now better define the mixing of the three groundwater types (N , F and D). The N type water derives its geochemistry from the shallow volcanic succession of the plain and mixes with F type carbonate groundwater that laterally discharges from Mt. Maggiore. These components are variably mixed with highly mineralized and CO_2 -rich type D water that migrates upward along normal faults throughout the region. The resulting geochemical composition in the *Ferrarele* wells are derived from the relative ratio between the three endmembers.

The Figure 1c graphically displays the physical mechanisms that can accommodate the mixing dynamics described above. The relative abundance of the D endmember corresponds with proximity of the groundwater well to normal faults. Secondary influences on the D endmember relate to the depth of the borehole relative to underlying stratigraphic changes demonstrated by increasing salinity gradients with depth. The F component is related to the carbonate aquifer

of Mt. Maggiore. The influence of this component on groundwater chemistry in the FGS depends upon the proximity of the outcrop to carbonate units and the depth of the monitoring well. According to the computed fractions and the cross sections in Figure 1c, the F component is relevant in less deep wells, with a bottom elevation comparable to the F monitoring point. It is likely that there is some density stratification between the dense D and the F or N endmember components. The N endmember components is representative of the less mineralized volcanically influenced groundwater; thus its composition is inversely proportional to the contributions of the D and F endmember components.

Detailed differences between each monitoring point may also depend on the structure of the groundwater well (e.g., location of the screens, the mean pumping rate, etc.) and on the local structural settings. The available hydrogeological and geochemical conceptual models, coupled with the large dataset of the *Ferrarele* area, promote this site as an optimal experimental site for scientific research on mixing hydrological processes involving mineral waters.

6 | CONCLUSIONS

A new method to quantify three endmember mixing was successfully applied in a mineralized groundwater system in southern Italy. The statistical methods used here can also be applied to future studies aiming to define contributions from different water sources. The availability of a dataset rich in variables allows a statistically robust evaluation of the most efficient geochemical tracers. Before the calculation of the endmembers fractions, it is mandatory to perform a detailed hydrogeochemical investigation, including the evaluation of main hydrogeochemical processes which could affect the chemical composition of the waters, and the analysis of the statistical distribution of variables which must not be normal or uni-modal to assess the tracer capability. Otherwise the quantification of the mixing fractions will be negatively affected by the lack of significant different concentration in the endmembers.

The inverse behaviour of the geochemical tracers in two endmembers and the independence of the third endmember allow a triangular configuration where each endmember is placed on a vertex and the sides represent the mixing function between two endmembers when the third one is equal to zero. Considering a generic water solution whose chemical composition is produced on the three-component mixing, data will be projected within the centre of the triangle (mixing subspace) with the mixing fractions detectable and quantifiable by homogeneous barycentric coordinates projections onto the sides of the triangle. The barycentric coordinates of the points corresponds to the algebraic computing of the three mixing fractions. The proposed method was validated comparing the calculated mixing fractions with the results of the EMMA computation on the same dataset.

The application of the geometrical method allow the validation of the three-component mixing model proposed in literature for the FGS, and the quantification of each aquifer (endmember) contribution.

The results improve also the knowledge on the contribution of shallow aquifers, which should be necessary taken in account in a sustainable exploitation plan.

ACKNOWLEDGEMENT

Open Access Funding provided by Istituto Nazionale di Geofisica e Vulcanologia within the CRUI-CARE Agreement. [Correction added on 18 May 2022, after first online publication: CRUI funding statement has been added.]

DATA AVAILABILITY STATEMENT

Datasets for this research are available in these in-text data citation references: Cuoco, Viaroli, Darrah, et al. (2021). <https://doi.org/10.4121/14216519.v1>

ORCID

Emilio Cuoco  <https://orcid.org/0000-0002-4637-1814>

Stefano Viaroli  <https://orcid.org/0000-0002-2521-7463>

REFERENCES

- Ahmad, A., van der Wal, B., Bhattacharya, P., & van Genuchten, C. M. (2019). Characteristics of Fe and Mn bearing precipitates generated by Fe(II) and Mn(II) co-oxidation with O₂, MnO₄ and HOCl in the presence of groundwater ions. *Water Research*, *161*, 505–516. <https://doi.org/10.1016/j.watres.2019.06.036>
- Albarède, F. (2009). *Geochemistry: An Introduction*. (2nd Edn.), Cambridge: Cambridge University Press. <https://doi.org/10.1017/CBO9780511807435>
- Appelo, C., & Postma, D. (2005). *Geochemistry, groundwater and pollution* (2nd ed.). Balkema Publishers.
- Barros Grace, V., Mas-Pla, J., Oliveira Novais, T., Sacchi, E., & Zuppi, G. M. (2008). Hydrological mixing and geochemical processes characterization in an estuarine/mangrove system using environmental tracers in Babitonga Bay (Santa Catarina, Brazil). *Continental Shelf Research*, *28*(4–5), 682–695. <https://doi.org/10.1016/j.csr.2007.12.006>
- Boncio, P., Dichiarante, A. M., Auciello, E., Saroli, M., & Stoppa, F. (2016). Normal faulting along the western side of the Matese Mountains: Implications for active tectonics in the central Apennines (Italy). *Journal of Structural Geology*, *82*, 16–36. <https://doi.org/10.1016/j.jsg.2015.10.005>
- Boni, C., Bono, P., & Capelli, G. (1986). Schema idrogeologico dell'Italia Centrale. *Mémoires de la Société Géologique Italiana*, *35*(2), 991–1012.
- Bundschuh, J., & Maity, J. P. (2015). Geothermal arsenic: Occurrence, mobility and environmental implications. *Renewable and Sustainable Energy Reviews*, *42*, 1214–1222. <https://doi.org/10.1016/j.rser.2014.10.092>
- Burns, D. A., McDonnell, J. J., Hooper, R. P., Peters, N. E., Freer, J. E., Kendall, C., & Beven, K. (2001). Quantifying contributions to storm runoff through end-member mixing analysis and hydrologic measurements at the Panola Mountain Research Watershed (Georgia, USA). *Hydrological Processes*, *15*(10), 1903–1924. <https://doi.org/10.1002/hyp.246>
- Capelli, G., Mazza, R., Trigari, A., & Catalani, F. (1999). *Le risorser idriche sotterranee strategiche nel distretto vulcanico di Roccamonfina (Campania nordoccidentale)*. Pitagora Ed, Bologna.
- Celico, P. (1978). Schema idrogeologico dell'Appennino carbonatico centro-meridionale. *Memorie e Note Istituto di Geologia Applicata*, *14*, 1–97.
- Christophersen, N., Neal, C., Hooper, R. P., Vogt, R. D., & Andersen, S. (1990). Modeling stream water chemistry as a mixture of soil water end-members—A step towards second-generation acidification models. *Journal of Hydrology*, *116*, 307–320. [https://doi.org/10.1016/0022-1694\(90\)90130-P](https://doi.org/10.1016/0022-1694(90)90130-P)
- Christophersen, N., & Hooper, R. P. (1992). Multivariate analysis of stream water chemical data: The use of principal components analysis for the end-member mixing problem. *Water Resources Research*, *28*(1), 99–107. <https://doi.org/10.1029/91WR02518>
- Corniello, A., Cardellicchio, N., Cavuoto, G., Cuoco, E., Ducci, D., Minissale, A., Mussi, M., Petruccione, E., Pelosi, N., Rizzo, E., Polemio, M., Tamburrino, S., Tedesco, D., Tiano, P., & Iorio, M. (2015). Hydrogeological characterization of a geothermal system: The case of the thermo-mineral area of Mondragone (Campania, Italy). *International Journal of Environmental Research*, *9*(2), 523–534. <https://doi.org/10.22059/IJER.2015.926>
- Cosentino, D., Federici, I., Cipollari, P., & Gliozzi, E. (2006). Environments and tectonic instability in Central Italy (Garigliano basin) during the late Messinian Lago–Mare episode: New data from the onshore Mondragone 1 well. *Sedimentary Geology*, *188–189*, 297–317. <https://doi.org/10.1016/j.sedgeo.2006.03.010>
- Coyte, R. M., & Vengosh, A. (2020). Factors controlling the risks of co-occurrence of the redox-sensitive elements of arsenic, chromium, vanadium, and uranium in groundwater from the eastern United States. *Environmental Science & Technology*, *54*(7), 4367–4375. <https://doi.org/10.1021/acs.est.9b06471>
- Cuoco, E., Viaroli, S., Darrah, T. H., Paolucci, V., Mazza, R., & Tedesco, D. (2021). Data underlying the article: A geometrical method for quantifying mixing fractions in three-component groundwater mixing: Experimental evidence from Ferrarelle aquifers. *4TU.ResearchData. Dataset*. <https://doi.org/10.4121/14216519.v1>
- Cuoco, E., Viaroli, S., Paolucci, V., Mazza, R., & Tedesco, D. (2021). Fe and As geochemical self-removal dynamics in mineral waters: Evidence from the Ferrarelle groundwater system (Riardo Plain, Southern Italy). *Environmental Geochemistry and Health*. In press. <https://doi.org/10.1007/s10653-021-00891-5>
- Cuoco, E., Verrengia, G., De Francesco, S., & Tedesco, D. (2010). Hydrogeochemistry of Roccamonfina volcano (Southern Italy). *Environment and Earth Science*, *61*, 525–538. <https://doi.org/10.1007/s12665-009-0363-3>
- Cuoco, E., Darrah, T. H., Buono, G., Eymold, W. K., & Tedesco, D. (2015). Differentiating natural and anthropogenic impacts on water quality in a hydrothermal coastal aquifer (Mondragone Plain, Southern Italy). *Environmental Earth Sciences*, *73*(11), 7115–7134. <https://doi.org/10.1007/s12665-014-3892-3>
- Cuoco, E., Darrah, T. H., Buono, G., Verrengia, G., De Francesco, S., Eymold, W. K., & Tedesco, D. (2015). Inorganic contaminants from diffuse pollution in shallow groundwater of the Campanian Plain (Southern Italy). Implications for geochemical survey. *Environmental Monitoring and Assessment*, *187*, 46. <https://doi.org/10.1007/s10661-015-4307-y>
- Cuoco, E., Minissale, A., Leo, D., Magda, A., Tamburrino, S., Iorio, M., & Tedesco, D. (2017). Fluid geochemistry of the Mondragone hydrothermal systems (southern Italy): Water and gas compositions vs. geostructural setting. *International Journal of Earth Sciences*, *106*(7), 2429–2444. <https://doi.org/10.1007/s00531-016-1439-4>
- Cuoco, E., Sacchi, E., De Francesco, S., Paolucci, V., Maletic, E. L., Darrah, T. H., Sirna, M., & Tedesco, D. (2020). Groundwater mixing in a heterogeneous multilayer aquifer driven by geogenic CO₂ fluxes: Evidence from chemical and isotopic composition of Ferrarelle waters (Riardo Plain, southern Italy). *Applied Geochemistry*, *116*, 104564. <https://doi.org/10.1016/j.apgeochem.2020.104564>
- D'Argenio, B., & Pescatore, T. (1962). Stratigrafia del Mesozoico nel gruppo del Monte Maggiore (Caserta). *Bollettino della Società dei Naturalisti in Napoli*, *71*, 55–61.
- De Vita, P., Allocca, V., Celico, F., Fabbrocino, S., Mattia, C., Monacelli, G., Musilli, I., Piscopo, V., Scalise, A. R., Summa, G., Tranfaglia, G., & Celico, P. (2018). Hydrogeology of continental southern Italy. *Journal*

- of *Maps*, 14(2), 230–241. <https://doi.org/10.1080/17445647.2018.1454352>
- Domenico, P. A., & Schwartz, F. W. (1997). *Physical and chemical hydrogeology* (2nd ed.). John Wiley & Sons, Inc.
- Donato, A., Tassi, F., Pecoraino, G., Manzella, A., Vaselli, O., Gagliano Candela, E., Santilano, A., La Pica, L., Scaleta, C., & Capecchiacci, F. (2021). Geochemical investigations of the geothermal systems from the Island of Sicily (southern Italy). *Geothermics*, 95, 102120. <https://doi.org/10.1016/j.geothermics.2021.102120>
- Dowling, C. B., Poreda, R. J., Basu, A. R., Peters, S. L., & Aggarwal, P. K. (2002). Geochemical study of arsenic release mechanisms in the Bengal basin groundwater. *Water Resources Research*, 38(9), 121–1218. <https://doi.org/10.1029/2001WR000968>
- Drever, J. (1997). *The geochemistry of natural waters*. Prentice Hall.
- Elsenbeer, H., Lorieri, D., & Bonell, M. (1995). Mixing model approaches to estimate storm flow sources in an overland flow-dominated tropical rain Forest catchment. *Water Resources Research*, 31(9), 2267–2278. <https://doi.org/10.1029/95WR01651>
- Gambardella, B., Marini, L., & Baneschi, I. (2005). Dissolved potassium in the shallow groundwaters circulating in the volcanic rocks of Central-Southern Italy. *Applied Geochemistry*, 20(5), 875–897. <https://doi.org/10.1016/j.apgeochem.2004.12.001>
- Genereux, D. (1998). Quantifying uncertainty in tracer-based hydrograph separations. *Water Resources Research*, 34(4), 915–919. <https://doi.org/10.1029/98WR00010>
- Giordano, G., Naso, G., Scrocca, D., Funicello, R., & Catalani, F. (1995). Processi di estensione e circolazione di fluidi a bassa termalità nella Piana di Riardo (Caserta, Appennino centro-meridionale). *Bollettino Società Geologica Italiana*, 144, 361–371.
- Harkness, J. S., Darrah, T. H., Moore, M. T., Whyte, C. J., Mathewson, P. D., Cook, T., & Vengosh, A. (2017). Naturally occurring versus anthropogenic sources of elevated molybdenum in groundwater: Evidence for Geogenic contamination from Southeast Wisconsin, United States. *Environmental Science & Technology*, 51, 12190–12199. <https://doi.org/10.1021/acs.est.7b03716>
- Hendry, M. J., Wassenaar, L. I., & Kotzer, T. (2000). Chloride and chlorine isotopes ($\delta^{36}\text{Cl}$ and $\delta^{37}\text{Cl}$) as tracers of solute migration in a thick, clay-rich aquitard system. *Water Resources Research*, 36(1), 285–296. <https://doi.org/10.1029/1999WR900278>
- Hooper, R. P., Christophersen, N., & Peters, N. E. (1990). Modeling stream water chemistry as a mixture of soil water end-members—An application to the Panola mountain catchment, Georgia, U.S.A. *Journal of Hydrology*, 116, 321–343. [https://doi.org/10.1016/0022-1694\(90\)90130-P](https://doi.org/10.1016/0022-1694(90)90130-P)
- Hooper, R. P. (2003). Diagnostic tools for mixing models of stream water chemistry. *Water Resources Research*, 39(3), HWC21–HWC213. <https://doi.org/10.1029/2002wr001528>
- Inamdar, S. (2011). The use of geochemical mixing models to derive runoff sources and hydrologic flow paths. In D. Levia, D. Carlyle-Moses, & T. Tanaka (Eds.), *Forest Hydrology and Biogeochemistry. Ecological Studies (Analysis and Synthesis). Ecological Studies*, (Vol. 216, pp. 163–183). Dordrecht: Springer. https://doi.org/10.1007/978-94-007-1363-5_8
- James, A. L., & Roulet, N. T. (2006). Investigating the applicability of end-member mixing analysis (EMMA) across scale: A study of eight small, nested catchments in a temperate forested watershed. *Water Resources Research*, 42(8), 1–17. <https://doi.org/10.1029/2005wr004419>
- Joreskog, K. G., Klován, J. E., & Reymont, R. A. (1976). *Geological factor analysis*. Elsevier.
- Katsuyama, M., Ohte, N., & Kobashi, S. (2001). A three-component end-member analysis of streamwater hydrochemistry in a small Japanese forested headwater catchment. *Hydrological Processes*, 15(2), 249–260. <https://doi.org/10.1002/hyp.155>
- Kehew, A. E. (2001). *Applied chemical hydrogeology* (1st ed.). Prentice-Hall.
- Kronholm, S. C., & Capel, P. D. (2014). A comparison of high-resolution specific conductance-based end-member mixing analysis and a graphical method for baseflow separation of four streams in hydrologically challenging agricultural watersheds. *Hydrological Processes*, 29(11), 2521–2533. <https://doi.org/10.1002/hyp.10378>
- Lancia, M., Petitta, M., Zheng, C., & Saroli, M. (2020). Hydrogeological insights and modelling for sustainable use of a stressed carbonate aquifer in the Mediterranean area: From passive withdrawals to active management. *Journal of Hydrology: Regional Studies*, 32, 100749. <https://doi.org/10.1016/j.ejrh.2020.100749>
- Langmuir, D. (1997). *Aqueous environmental geochemistry*. Prentice-Hall, Inc.
- Li, P., Karunanidhi, D., Subramani, T., & Srinivasamoorthy, K. (2021). Sources and consequences of groundwater contamination. *Archives of Environmental Contamination and Toxicology*, 80(1), 1–10. <https://doi.org/10.1007/s00244-020-00805-z>
- Lidberg, P. (2011). *Barycentric and Wachspress coordinates in two dimensions: Theory and implementation for shape transformations* (U.U.D.M. Project report 2011:3), 37pp. Uppsala University.
- Liu, F., Bales, R. C., Conklin, M. H., & Conrad, M. E. (2008). Stream flow generation from snowmelt in semi-arid, forested and seasonally snow-covered catchments, Valles Calder, New Mexico. *Water Resources Research*, 44, W12443. <https://doi.org/10.1029/2007WR006278>
- Liu, F., Conklin, M. H., & Shaw, G. D. (2017). Insights into hydrologic and end-member mixing processes based on concentration-discharge and end-member mixing analyses in the mid-Merced River Basin, Sierra Nevada, California. *Water Resources Research*, 53(1), 832–850. <https://doi.org/10.1002/2016WR019437>
- Long, G. L., & Winefordner, J. D. (1983). Limit of detection: A closer look at the IUPAC definition. *Analytical Chemistry*, 55, 712–724. <https://doi.org/10.1021/ac00258a001>
- Luhr, J. F., & Giannetti, B. (1987). The Brown Leucitic Tuff of Roccamonfina Volcano (Roman Region, Italy). *Contributions to Mineralogy and Petrology*, 95, 420–436. <https://doi.org/10.1007/BF00402203>
- Mateo-Sagasta, J., Zadeh, S. M., Turrall, H., & Burke, J. (2017). *Water pollution from agriculture: A global review. Executive summary*. Rome, Italy: FAO; Colombo, Sri Lanka: International Water Management Institute (IWMI). CGIAR Research Program on Water, Land and Ecosystems (WLE), 35p.
- Mazor, E., Drever, J. I., Finley, J., Huntoon, P. W., & Lundy, D. A. (1993). Hydrochemical implications of groundwater mixing: An example from the Southern Laramie Basin, Wyoming. *Water Resources Research*, 29(1), 193–205. <https://doi.org/10.1029/92WR01680>
- Mazza, R., Pietrosante, A., Taviani, S., & Viaroli, S. (2013). A preliminary understanding of groundwater exchanges between the Riardo Plain and Mount Maggiore ridge (Campania, Italy). *Rendiconti Online Società Geologica Italiana*, 24, 207–209.
- Ogunkoya, O. O., & Jenkins, A. (1993). Analysis of storm hydrograph and flow pathways using a three-component hydrograph separation model. *Journal of Hydrology*, 142(1–4), 71–88. [https://doi.org/10.1016/0022-1694\(93\)90005-t](https://doi.org/10.1016/0022-1694(93)90005-t)
- Osemwegie, I., Stumpp, C., Biemi, J., & Reichert, B. (2018). Multi-tracer assessment of seasonal water source changes in coastal water systems along the southeastern coast of Ivory Coast (West Africa). *Hydrological Sciences Journal*, 63(15–16), 2124–2145. <https://doi.org/10.1080/02626667.2018.155836>
- Parkhurst, D. L., & Appelo, C. A. J. (1999). *User's guide to PHREEQC (Version 2)—A computer program for speciation, batch-reaction, one-dimensional transport, and inverse geochemical calculations* (U.S. Geological Survey Water-Resources Investigations Report 99-4259), p. 310.
- Pelizzardi, F., Bea, S. A., Carrera, J., & Vives, L. (2017). Identifying geochemical processes using end member mixing analysis to decouple chemical components for mixing ratio calculations. *Journal of Hydrology*, 550, 144–156. <https://doi.org/10.1016/j.jhydrol.2017.04.010>

- Ramón, J., Correa, A., Timbe, E., Mosquera, G. M., Mora, E., & Crespo, P. (2021). Do mixing models with different input requirement yield similar streamflow source contributions? Case study: A tropical montane catchment. *Hydrological Processes*, 35(6), 1–17. <https://doi.org/10.1002/hyp.14209>
- Rashad, M. M., Radwan, M., & Hessian, M. (2008). Effect of Fe/Ba mole ratios and surface-active agents on the formation and magnetic properties of co-precipitated barium hexaferrite. *Journal of Alloys and Compounds*, 453(1–2), 304–308. <https://doi.org/10.1016/j.jallcom.2006.11.080>
- Renner, R. M. (1988). *On the resolution of compositional data sets into convex combinations of extreme vectors* (Technical Report No. 88/02), 48 pp., Institute of Statistics and Operations Research, Victoria University of Wellington, New Zealand
- Rutherford, J. C. (1994). *River mixing*. Chichester England: Wiley.
- Sacchi, E., Cuoco, E., Oster, H., Paolucci, V., Tedesco, D., & Viaroli, S. (2021). Tracing groundwater circulation in a valuable mineral water basin with geochemical and isotopic tools: The case of FERRARELLE, Riardo basin, Southern Italy. *Environmental Geochemistry and Health*. In press. <https://doi.org/10.1007/s10653-021-00845-x>
- Schramke, J. A., Murphy, E. M., & Wood, B. D. (1996). The use of geochemical mass-balance and mixing models to determine groundwater sources. *Applied Geochemistry*, 11(4), 523–539. [https://doi.org/10.1016/0883-2927\(96\)00007-8](https://doi.org/10.1016/0883-2927(96)00007-8)
- Saroli, M., Lancia, M., Albano, M., Mondoni, G., Moro, M., & Scarascia Mugnozza, G. (2014). New geological data on the Cassino intramontane basin, central Apennines, Italy. *Rendiconti Lincei*, 25(2), 189–196. <https://doi.org/10.1007/s12210-014-0338-5>
- Shaheen, S. M., Alessi, D. S., Tack, F. M. G., Ok, Y. S., Kim, K. H., Gustafsson, J. P., Sparks, L., & Rinklebe, J. (2019). Redox chemistry of vanadium in soils and sediments: Interactions with colloidal materials, mobilization, speciation, and relevant environmental implications—A review. *Advances in Colloid and Interface Science*, 265, 1–13. <https://doi.org/10.1016/j.cis.2019.01.002>
- Stegen, J. C., Fredrickson, J. K., Wilkins, M. J., Konopka, A. E., Nelson, W. C., Arntzen, E. V., Chrisler, W. B., Chu, R. K., Danczak, R. E., Fansler, S. J., Kennedy, D. W., Resch, C. T., & Tfaily, M. (2016). Groundwater-surface water mixing shifts ecological assembly processes and stimulates organic carbon turnover. *Nature Communications*, 7, 11237. <https://doi.org/10.1038/ncomms11237>
- Stumm, W., & Morgan, J. J. (1996). *Aquatic chemistry: Chemical equilibria and rates in natural waters*. Wiley-Interscience Publication <https://trove.nla.gov.au/work/31691612>
- Szulczewski, W., & Jakubowski, W. (2018). The application of mixture distribution for the estimation of extreme floods in controlled catchment basins. *Water Resources Management*, 32(10), 3519–3534. <https://doi.org/10.1007/s11269-018-2005-6>
- Tassi, F., Vaselli, O., Tedesco, D., Montegrossi, G., Darrah, T., Cuoco, E., Mapendano, M. Y., Poreda, R., & Delgado Huertas, A. (2009). Water and gas chemistry at Lake Kivu (DRC): Geochemical evidence of vertical and horizontal heterogeneities in a multibasin structure. *Geochemistry, Geophysics, Geosystems*, 10(2), 1–22. <https://doi.org/10.1029/2008gc002191>
- Università degli Studi Roma Tre (1996). Studio petrografico di alcuni campioni prelevati da carote di pozzo nell'area della concessione "Ferrarelle" situata nei pressi di Riardo (CE) - Relazione finale. Unpublished technical report. p. 49.
- Viaroli, S., Mastroiello, L., Mazza, R., & Paolucci, V. (2016). Hydrostructural setting of Riardo plain: Effects on Ferrarelle mineral water type. *Acque Sotterranee*, 5(3), 59–68. <https://doi.org/10.7343/as-2016-226>
- Viaroli, S., Mastroiello, L., Lotti, F., Paolucci, V., & Mazza, R. (2018). The groundwater budget: A tool for preliminary estimation of the hydraulic connection between neighboring aquifers. *Journal of Hydrology*, 556, 72–86. <https://doi.org/10.1016/j.jhydrol.2017.10.066>
- Viaroli, S., Lotti, F., Mastroiello, L., Paolucci, V., & Mazza, R. (2019). Simplified two-dimensional modelling to constrain the deep groundwater contribution in a complex mineral water mixing area, Riardo Plain, southern Italy. *Hydrogeology Journal*, 27, 1459–1478. <https://doi.org/10.1007/s10040-018-1910-3>
- Viaroli, S., Di Curzio, D., Lepore, D., & Mazza, R. (2019). Multiparameter daily time-series analysis to groundwater recharge assessment in a caldera aquifer: Roccamonfina Volcano, Italy. *Science of the Total Environment*, 676, 501–513. <https://doi.org/10.1016/j.scitotenv.2019.04.327>
- Warner, N. R., Jackson, R. B., Darrah, T. H., Osborn, S. G., Down, A., Zhao, K. G., White, A., & Vengosh, A. (2012). Geochemical evidence for possible natural migration of Marcellus Formation brine to shallow aquifers in Pennsylvania. *Proceedings of the National Academy of Sciences of the United States of America*, 109, 11961–11966.
- Wilson, A. M., Williams, M. W., Kayastha, R. B., & Racoviteanu, A. (2016). Use of a hydrologic mixing model to examine the roles of meltwater, precipitation and groundwater in the Langtang River basin, Nepal. *Annals of Glaciology*, 57(71), 155–168. <https://doi.org/10.3189/2016aog71a067>

How to cite this article: Cuoco, E., Viaroli, S., Darrah, T. H., Paolucci, V., Mazza, R., & Tedesco, D. (2021). A geometrical method for quantifying endmembers' fractions in three-component groundwater mixing. *Hydrological Processes*, 35(11), e14409. <https://doi.org/10.1002/hyp.14409>